Received: 22 July 2024 | Revised: 25 September 2024 | Accepted: 26 November 2024 | Published online: 3 December 2024

RESEARCH ARTICLE

Journal of Optics and Photonics Research
2024, Vol. 00(00) 1–8
DOI: 10.47852/bonviewJOPR42023911

BON VIEW PUBLISHING

Green Synthesis of Noble Metal Nanoparticles: Nonlinear Optics and Applications

Fryad Z. Henari[1],* and G. Roshan Deen[1]

[1]*Department of Medical Sciences, Royal College of Surgeons in Ireland – Bahrain, Bahrain*

Abstract: This study presents a green method for synthesizing gold nanoparticles (AuNPs) and silver nanoparticles (AgNPs) employing Gum Arabic extract as a reducing and stabilizing agent. The synthesized nanoparticles are characterized using UV-Vis absorption spectroscopy and transmission electron microscopy (TEM). The visible color change and the presence of surface plasmon resonance (SPR) peaks confirmed the formation of silver and gold nanoparticles. The size of the nanoparticles was determined from the UV-Vis spectra data, and the results were compared to sizes measured by TEM. The nonlinear refraction (n_2) and nonlinear absorption (β) coefficient of AgNPs and AuNPs at 488 and 514 nm were investigated under continuous wave mode excitation using the Z-scan technique. By fitting the experimental data to the Z-scan theoretical equations, the nonlinear refraction index and the nonlinear absorption coefficient were found. The origin of the nonlinearities was discussed, and it was proposed to be of thermal effect for the nonlinear refractive index and reverse saturation absorption for nonlinear absorption. Optical limiting and switching were demonstrated by taking advantage of the samples' nonlinear optical characteristics.

Keywords: Gum Arabic, gold-silver nanoparticles, particle size calculation, nonlinear property, optical limiting, optical switching

1. Introduction

Nanoparticles (NPs) have been widely studied due to their distinctive physical and chemical properties primarily arising from their dimensions (1–100 nm). These properties make them suitable for many scientific and medical applications [1], including optoelectronics [2], optical limiting, optical switching [3], thermal therapy, photodynamic [4, 5], and drug delivery [6]. The NPs' surface plasmon resonance (SPR) is responsible for their unique optical characteristics. SPR is coupled with the oscillation of electrons on the conduction band surface of NPs triggered by the incident light frequency that coincides with the electrons' plasma frequency. The incident wavelength at the SPR band and its vicinity significantly enhances the optical and nonlinear optical properties of NPs [7]. The property of SPR strongly depends on the shape, size, composition, and dielectric environment [8], and this property makes the NPs promising candidates for various applications in nonlinear optics, such as frequency mixing [9], optical limiting, and optical switching [3, 10, 11].

The techniques used for synthesizing NPs are either by chemical or physical methods. The chemical processes are based on applying different chemical-reducing and stabilizing precursor agents. Most chemical-reducing agents can present severe risks to health and environment-related issues [12, 13]. The physical methods often involve high temperature, high pressure, and complex equipment, such as lasers and chemical evaporation processes, making them expensive and posing safety issues if the equipment is not appropriately handled. On the other hand, the green synthesis of NPs is a method that is less harmful to the environment. It offers a more straightforward method, less toxicity, and cost-effectiveness than chemical and physical methods, and it is often performed at ambient temperature and pH.

Natural capping and reducing agents found in plant and microorganism biological extracts are used in the green synthesis process. A range of biological extracts, including yeast, fungi, bacteria, fruit, and plant, has gained considerable interest, where the phytochemical molecules are present, such as sugars, amino acids, lipids, polyphenols, terpenoids, alkaloids, phenolic compounds, and proteins playing an essential part as the reducing and stabilizing agents. NPs have been synthesized using a variety of plant extracts, such as olive oil, tea, okra, and types of hibiscus, as well as commercially available plant products such as curcumin, cinnamon, and Gum Arabic (GA) [14, 15]. GA is a polymeric material exuded from trees, like Acacia Senegal, which is composed of glycoprotein and polysaccharide. Through chemical reactions, the polymer chains with hydroxyl groups and amino acids might convert metal ions into metal NPs [16–18].

In this work, GA extract was used to synthesize AuNPs and AgNPs. The existence of distinctive SPR bands in the absorption spectra verified the production of AuNPs and AgNPs. The absorbance ratio at the SPR peak wavelength and the absorbance of the lower wavelength prior to the SPR band peak were used to estimate the sizes of the synthesized NPs from the UV-Vis absorption spectra. The average size measurements derived from

*Corresponding author: Fryad Z. Henari, Department of Medical Sciences, Royal College of Surgeons in Ireland – Bahrain, Bahrain. Email: fzhenari@rcsi-mub.com

the transmission electron microscopy (TEM) images were contrasted with the estimated sizes of the NPs.

The Z-scan technique, at wavelengths of 488 nm and 514 nm, was used to investigate the nonlinear optical characteristics of the AuNPs and AgNPs, including their nonlinear refractive index and nonlinear absorption coefficient. The sample's nonlinear optical characteristics are used to demonstrate optical switching and limiting. The origin of these effects is explained. The results from this study reveal that green-synthesized AgNPs and AuNPs are promising nonlinear materials with potential applications in photonic applications and optical switches. To our knowledge, AuNPs and AgNPs synthesized using GA have not been fully explored for nonlinear properties at the wavelength used in this study.

2. Materials and Methods

2.1. Materials

Acacia tree GA, sodium hydroxide, gold (III) chloride trihydrate (HAuCl4), and silver nitrate (AgNO3) were all acquired from Sigma-Aldrich and used as supplied. The solutions were made using deionized water from a Millipore system.

2.2. Synthesis of gold nanoparticles

0.375 g of GA and 25 ml of deionized water were combined to create a 15 g/l GA solution. Whatman No. 1 filter paper was then used to filter the combination. Gold, and silver NP samples were synthesized by mixing different $HAuCl_4$ (1 mM) and $AgNO_3$ (1 mM). Different volumes of the solution mixed with a fixed volume of GA solution at room temperature. Following ten seconds of heating in a 1000 W microwave oven, 100 µl of 0.5 M NaOH was added to each solution. NaOH is added to decrease the reduction time and keep the pH above the isoelectric point to increase the negativity of the surface charge, improve stability, and prevent aggregation [19]. The initial confirmation of gold and silver NP formation was indicated by a color change to deep purple (red) for gold and yellow for silver NPs, as illustrated in Figure 2 (inset). The synthesized NPs were centrifuged at 4500 rpm for 10 min, and the residue was washed with distilled water twice and dried in an oven at 60°C for 48 h. For further experiments, the dry powder was dispersed in distilled water.

2.3. Characterization

A Shimadzu UV-1800 spectrophotometer was used to detect the absorption spectra in order to pursue the formation of gold and silver NPs. After 30 min of preparation, the measurements were taken to give the reaction enough time to complete. The size and shape of the NPs were ascertained using TEM. These findings were compared with values obtained from Mie theory calculation, derived from the absorbance ratio at the SPR peak to the absorbance immediately preceding this peak. Possible interactions between AuNPs, AgNPs, and GA molecules that could aid in the reduction and capping of NPs were examined using FTIR measurements. Figure 1 illustrates preparing the GA-mediated synthesis of gold and silver NPs and measuring nonlinear optical properties.

2.4. Nonlinear optical studies

The Z-scan technique was used to examine the NPs' (AuNPs and AgNPs) nonlinear refractive index and nonlinear absorption coefficient [20]. The method is founded on the beam intensity variation as the sample is moved along the lens's focal region, with the focal point experiencing the highest intensity. A computerized stepping motor was used to move the sample along z-axis of the focal. The transmission through the samples at the farfield with and without an aperture was measured. These measurements distinguish between nonlinear absorption (open aperture) and nonlinear refractive index (closed aperture). A custom-built Z-scan setup was employed using an air-cooled continuous wave (CW) Argon ion laser at 488 and 514 nm with an average power of 20 mW. The laser beam was focused to 20 µm using a 5 cm focal length lens, achieving an intensity of 3.2×10^7 W m^{-2}.

The optical limiting process reduces the output transmission intensity through a material as the input intensity increases. At low incident intensities, the material has a linear transmittance;

Figure 1
An illustration showing how to prepare gold and silver nanoparticles and test their nonlinear optical characteristics

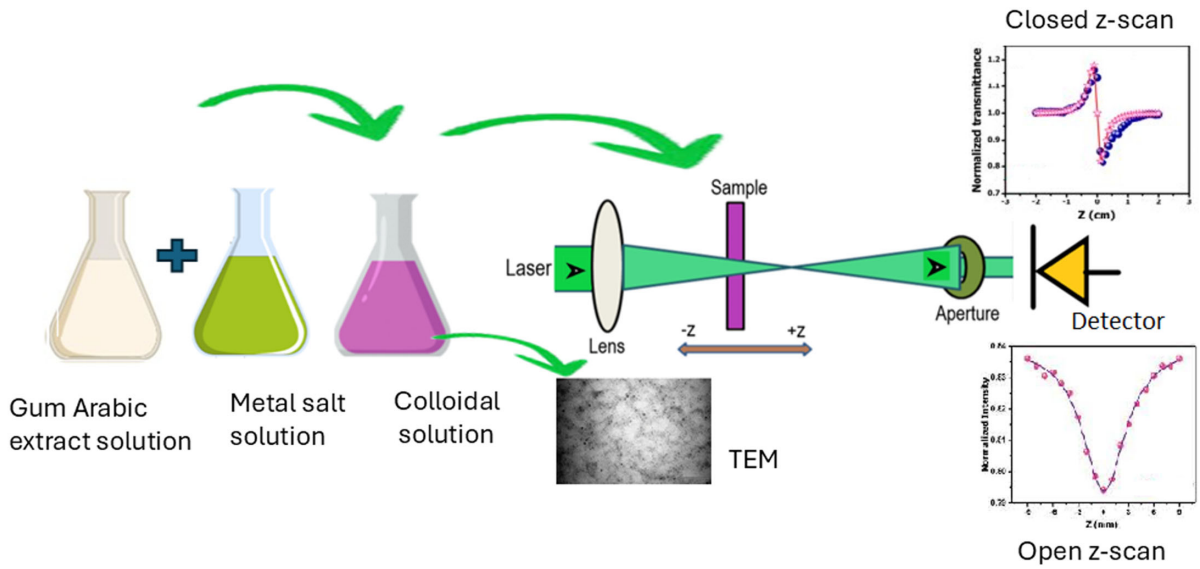

Figure 2
Absorption spectra for AgNPs and AuNPs. (Inset) photos of colloidal AgNPs and AuNPs

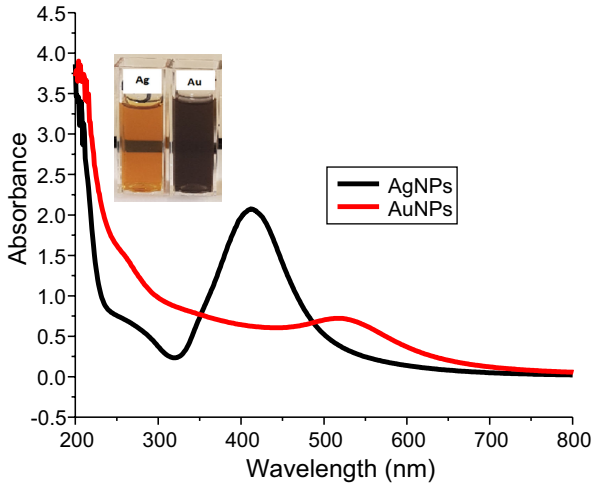

in contrast, at some high critical incident intensities, the transmission clamped and stayed at a constant value; this critical incident value is referred to as a threshold intensity that would be less than the intensity required to damage the material itself or components behind. The lower the threshold values, the better the material is as an optical limiter. This phenomenon can be used to protect detectors, switches, and human eyes from high-intensity laser beams. The optical limiting of AuNPs and AgNPs at 488 nm and 514 nm is examined in this work. In the Z-scan experiment, the sample was placed at the transmission minimum. The laser power input was changed using neutral density filters; the input and transmission power were recorded using a power meter.

Photonic switching behavior in AuNPS and AgNPs was observed using the pump and probe approach. A weak He-Ne laser beam ($\lambda = 633$, 1 mW) was employed as the probe, while the Argon ion laser beam ($\lambda = 488$ nm, 514 nm, 20 mW) was employed as the pump beam. Changes in the transmission of the samples caused by the pump were observed using the probe beam.

3. Results and Discussion

3.1. Optical property and size analysis of the nanoparticles

A fixed volume of Gum Arabic (GA) extract was combined with varying quantities of HAuCl4 (1 mM) and AgNO3 (1 mM) solutions was used to prepare samples of gold and silver NPs. The samples were heated in a microwave oven to speed up the chemical reduction process. After heating and adding NaOH, the color of the solution changed to purple for AuNPs and dark yellow for AgNPs, indicating the formation of NPs Figure 2(inset). The color shift is caused by the conduction band electrons oscillations in resonance with the incident photon frequency, which creates an absorption band called SPR [18]. The best results were obtained by mixing an equal volume of the extract with an equal volume of the salt.

The absorption spectra of produced gold and silver NPs are displayed in Figure 2. The spectra reveal the characteristic SPR bands with a single peak around 519 nm and 418 nm for AuNPs and AgNPs, respectively. The observed single SPR peak suggests that the NPs are almost spherical [21]. After a month, the samples' absorption spectra were examined, and the SPR peaks showed no change, suggesting that the NPs were stable.

The following formula was utilized to calculate the average size of the NPs based on their absorption spectra [22],

$$d = Exp\left(B_1 \frac{A_{spr}}{A_{450}} - B_2\right) \quad (1)$$

where d is the diameter of the particle, and B_1 and B_2 are experimentally determined fit parameters from plotting A_{spr}/A_{450} as a function of particle size diameter ($B_1 = 3.00$, $B_2 = 2.20$) [21], A_{spr} is the absorbance at SPR peak wavelength, and A_{450} is the absorbance of lower wavelength before the SPR band peak. The diameter of the particles was determined using the equation above, and it was 3.93 nm for AuNPs and 5 nm for AgNPs.

Figure 3 shows the morphology of the synthesized NP particles, analyzed using TEM. The images demonstrate that the NPs' main form is spherical. The size distribution of colloidal AuNPs and AgNPs was analyzed utilizing Image J1.5J software. The size distribution histogram in Figure 3 reveals an average size of around 4 nm for AuNPs and 5 nm for AgNPs. These values agree with the ones derived from the absorption. Therefore, NP size can be determined using the absorption spectra instead of the expensive TEM [22].

FTIR spectroscopy was used to investigate the possible interactions between AuNPs, AgNPs, and GA molecules, which are thought to be accountable for NP reduction and capping. The FTIR spectra of GA, GA-AuNPs, and GA-AgNPs are shown in Figure 4.

Prominent peaks at approximately 3340 cm^{-1} and 2925 cm^{-1} indicate N-H stretching vibration and C-H stretching groups, respectively. The band at 1610 cm^{-1} is associated with C-O-C and C-OH vibrations originating from GA's protein/polysaccharide components. The asymmetric stretching of the -COO- group is responsible for the peak at 1446 cm^{-1}. The spectral region between 1200 and 900 cm^{-1} is characteristic of carbohydrate (polysaccharide) structures. The peak at 867 cm^{-1} is assigned to the stretching vibration of C-O bonds within the GA-AuNP complex. The presence of these peaks in both GA and the NP mixtures provides strong evidence for NP formation. Furthermore, the small peak position shifts between the GA and GA-AuNPs spectra imply that the functional groups of GA interact with the NPs' charged surface.

3.2. Nonlinear properties of the synthesized nanoparticles

The nonlinear optical characteristics of the synthesized AuNPs and AgNPs are examined using the Z-scan technique. The normalized transmittance curve of a closed aperture for AuNPs and AgNPs is shown in Figure 5. The normalized transmission curve's observed pre-focal peak and post-focal valley suggest that the investigated NPs have a negative nonlinear refractive index ($n_2 < 0$). The CW form of the laser beam utilized in this study and the peak valley formation and non-symmetric nature of the reported Z-scan measurements suggest that thermal lensing processes, which lead to self-defocusing, are responsible for the observed nonlinear refractive index. Thermal lensing arises when the medium absorbs the laser beam, generating localized heat. This heat diffuses within the medium, creating non-uniform temperature distribution within the medium and, consequently, resulting in the variation of refractive index due to the refractive index dependence of temperature (dn/dT), which acts as a thermal lens, succeeding in the phase alteration of the beam. In this

Figure 3
(Top): TEM images and size distribution of colloidal Au nanoparticles with an average size of 5 nm. (Bottom) TEM images and size distribution of colloidal Ag nanoparticles with an average size of 4 nm, respectively

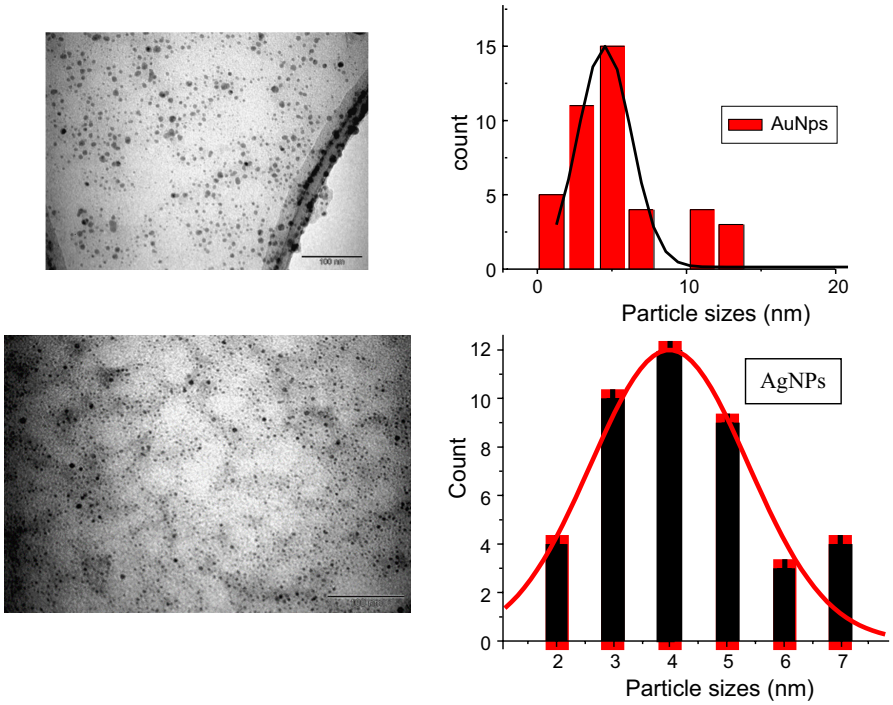

Figure 4
Normalized FTIR spectra of gum Arabic (Red), GA-AuNPs (black), and GA-AgNPs (blue)

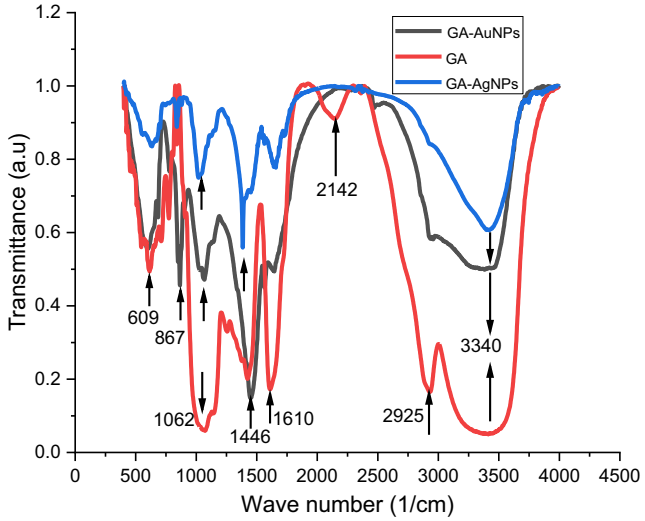

situation, the nonlinear response can be determined using the thermal lens model [23].

$$T = \left(1 + \frac{2x\,\varphi}{1+x^2} + \frac{\varphi^2}{1+x^2}\right)^{-1} \tag{2}$$

where φ is the nonlinear phase change, the diffraction length of the Gaussian beam is $x = \frac{z}{z_o}$ (with $z_o = \frac{\pi w_o^2}{\lambda}$), w_o is the beam waist at focus, and λ is the wavelength. The values of φ were obtained by fitting Equation (2) to the normalized closed aperture data.

The relationship between the nonlinear phase change φ and the nonlinear refractive index n_2 is as follows: [23]

$$n_2 = \frac{\varphi\alpha\lambda}{2\pi I_o\left(1 - e^{-\alpha l}\right)} \tag{3}$$

where α is the linear absorption coefficient, λ is the wavelength, I_o is the intensity at the focus, and l is the thickness of the sample.

The blue and red lines are the fit based on Equation (2) to the experimental data (black lines).

Equation (2) was used to fit the experimental results; displayed in Figure 5. Equation (3) was used to determine the values of the nonlinear refractive index n_2 based on the values of φ that were obtained from the fitting; the results are summarized in Table 1.

The samples' varying linear absorption at the wavelength utilized in the experiment could be the source of the slight variations in n_2. The absorption at 488 nm is higher for being close to the SPR peak of AgNPs; the value of n_2 at 488 nm is expected to be higher than the n_2 value for the AuNPs. Also, for 514 nm, the absorption is high for being close to the SPR peak of AuNPs, and the value of n_2 for AuNPs is expected to be higher than AgNPs.

The nonlinear refractive index values computed and published here are consistent with those reported by [24]. Leila Sarkhosh et al. [25] the nonlinear refractive index for AuNPs at cw 532 nm was measured and found it to be 1.58×10^{-7} cm^2/W, one order higher than the reported value. Comparing the quantitative results, however, could be of concern because the nonlinear response depends on the NPs' size, shape, concentration, and probed wavelength [26, 27].

Figure 5
Normalized transmittance obtained from closed aperture Z-scan for AgNPs at 514 nm and AuNPs at 488 nm

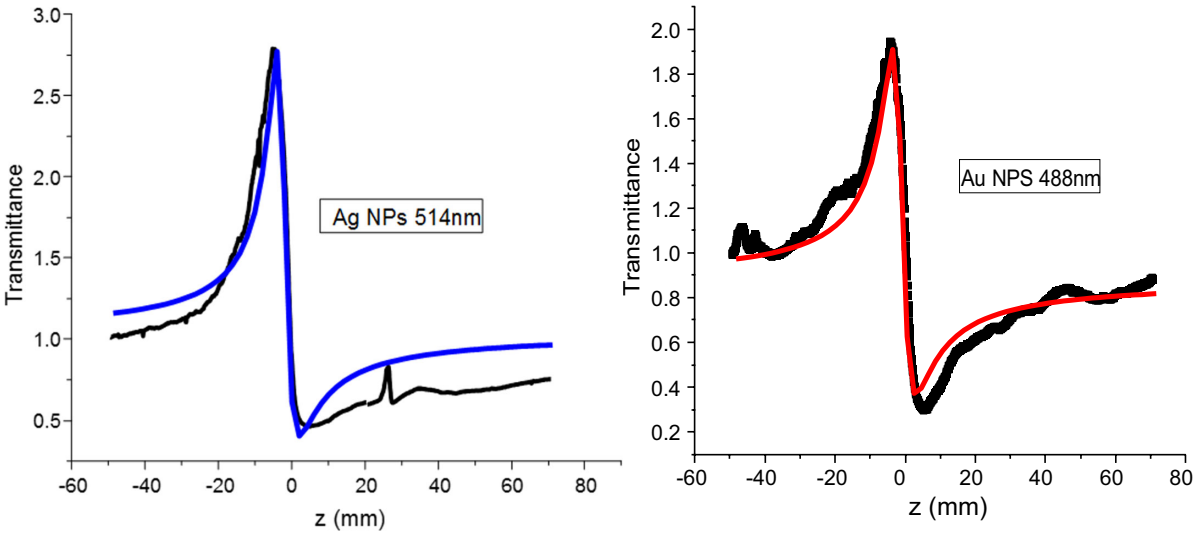

Table 1
Calculated n_2 and β values for AgNPs and AuNPs at wavelengths 488 nm and 514 nm

Sample	l (nm)	a/cm	b(cm/W)	n_2 (cm^2/W)
AgNPs	488	1.61	7.36×10^{-3}	3.2×10^{-8}
	514	1.38	5.80×10^{-3}	5.24×10^{-9}
AuNPs	488	1.01	7.15×10^{-3}	3.01×10^{-8}
	514	1.65	9.83×10^{-3}	6.90×10^{-8}

Figure 6
Normalized transmittance of open aperture Z-scan for AgNPs and AuNps at 514 nm. Black lines are the experimental data, and the blue and red lines are the fit of Equation 4

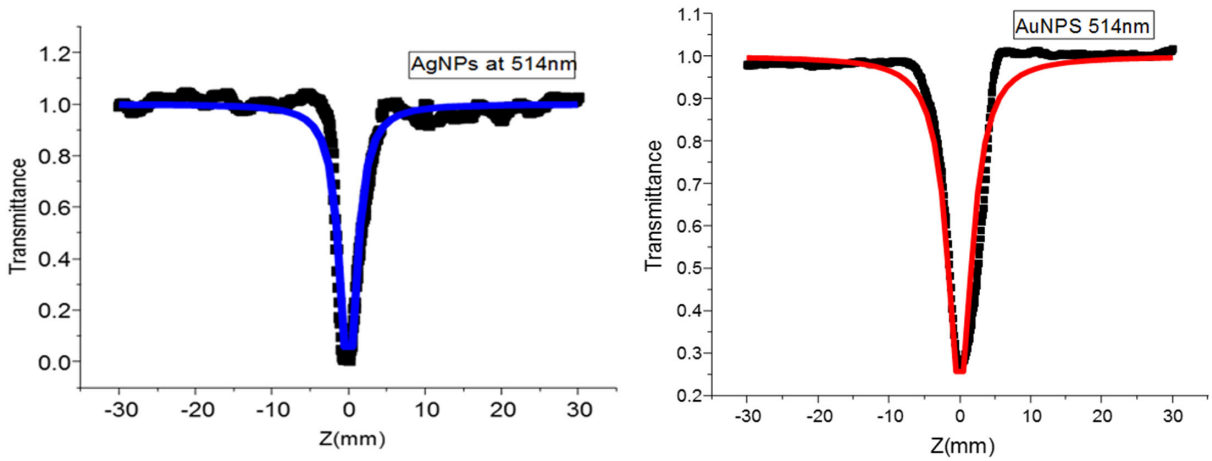

Figure 6 shows the normalized open aperture transmission of AuNPs and AgNPs at wavelengths of 488 nm and 514 nm. The samples' nonlinear absorption is reverse saturation absorption (RSA), as indicated by the minimal normalized transmission at the focus ($z = 0$). In general, the nonlinear absorption of NPs typically arises from free carriers generated by the intraband (sp→sp) and interband (d→sp) transitions and SPR response. The SPR response is the collective excitation of the conduction band electrons, which will be influential since the excitation wavelengths of 514 nm and 448 nm used in this study are located within the vicinity of SPR peak (nearly off-resonant), which results in a strong absorption.

Free carriers are produced when SPR decays via intraband and interband transitions. Additionally, direct intraband and interband excitations contribute to free carrier generation in the conduction

band. These free carriers, which come from band transitions and SPR decay, increase absorption cross sections, which in turn increase photon absorption from the laser beam and produce RSA [28].

The normalized transmission for open aperture Z-scan is [23]

$$T = 1 - \frac{\beta I_0 L_{eff}}{2\sqrt{2}\,(1 - x^2)} \tag{4}$$

where β is the nonlinear absorption coefficient, I_o is the intensity of the beam at focus, and *Leff* is effective absorption length and given by $= 1 - \exp(-\alpha l))/\alpha$, where α is a linear absorption coefficient, l is the sample thickness, and x is the diffraction length of the Gaussian beam $x = \frac{z}{z_o}$(with $z_o = \frac{\pi w_o^2}{\lambda}$), wo is the beam size at focus. Equation (4) was fitted to the experimental data to get the nonlinear absorption coefficient; the findings are also displayed in Table 1.

Elham et al. [29] measured the nonlinear absorption for AuNPs using a Z-scan at 637 nm cw and found it to be 4.46×10^{-4} cm^2/W; this value is ten times lower than the value reported here at 514 nm and 488 nm. The nonlinear absorption value of 10^{-3} cm/W for AgNPs reported by [30] is in the same order as the reported value in this study. As previously stated, comparing the quantitative values of nonlinear response may be of concern due to their reliance on the probed wavelength, NP size, shape, and concentration.

An Argon ion laser at 488 nm and 514 nm with an output power of 20 mW was used to investigate the optical limiting of the materials. A 1 mm cuvette was filled with colloidal solutions of gold and silver and was positioned in the open z-scan where the transmission was at its lowest. A variable neutral density filter was utilized to alter the laser beam's input power, and a power meter was used to record the sample's input and output powers. The sample's transmittance was monitored by measuring the outpower from the sample through an aperture as the laser input power was incrementally increased.

Figure 7 shows the transmission output power plotted against the input laser power for AuNPs and AgNPs (inset). The figures demonstrate that the output power varied linearly at low input power. The sample's output power departed from linearity at high input power. The optical limiting values were measured where the deviations occurred. Similar trends were observed for both samples at 488 nm and 514 nm. AgNPs and AuNPs reveal almost the same optical limiting efficiency with little differences depending on the wavelength used.

The AgNPs showed a better threshold limiting than AuNPs at 488 nm (for AgNPs at 488 is 16 mW, and for AgNPs at 514 nm is 17 mW); this is because the AgNP absorbs the light at 488 nm more efficiently since it resides closer to the SPR peak. While the AuNPs show better optical limiting than AgNPs at 514 nm (for AuNPs at 488 nm is 18 mW, and for AuNps at 514 nm is 16 mW); this is because the AuNPs absorb the light at 514 nm more efficiently since they are located closer to the SPR peak of gold NPs (Figure 2).

Several mechanisms, including free carrier absorption, two-photon absorption, reverse-saturable absorption, and nonlinear refraction, (self-focusing, self-defocusing), have been suggested to explain optical limiting [31]. Since the minimum transmission from the sample occurred at focus ($z = 0$) see Figure 6, as previously said, it may be inferred that reverse saturation absorption is responsible for the optical limiting mechanism displayed by the samples. However, the contribution of heating as a result of absorption cannot be neglected.

Photonic switching manipulates the output light beam by another light beam within the specific recovery time. The pump and probe measurements were employed to show photonic switching in AuNPS and AgNP samples. To measure the sample transmission induced by the pump beam, a low-power He-Ne laser (λ = 633, 1 mW) was used as the probe and an Argon ion laser beam (λ = 488 nm, 20 mW) as the pump beam. A lens is used to focus the collinear pump and probe beams on the sample. A narrow band filter separated the pump beam from the probe beam. In the Z-scan experiment, the sample was moved to a position where transmission is negligible (closed case). Modulation of the pump beam was done using a mechanical chopper. Photodiodes detected the pump and probe beam and showed on an oscilloscope. The waveform traces of the probe beam (lower trace) and the pump beam (upper trace) are displayed in Figure 8. The graphic illustrates optical inverted switching,

Figure 7
The optical limiting behavior for AuNPs and AgNPs at 488 nm and 514 nm. The threshold values are given in the text

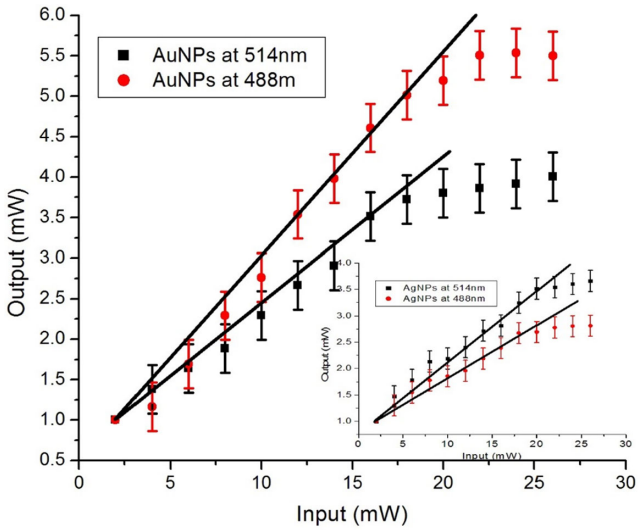

Figure 8
Pump (lower trace) and probe (upper trace) waveforms

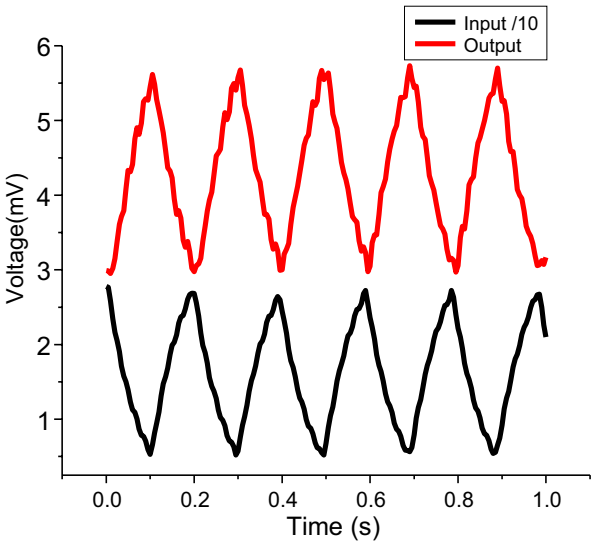

It can be seen from the figure when the probe beam is intensely absorbed and in a "off" state when the pump beam is in a "on" state. The inverting switching behavior is explained as follows: when the sample is exposed to the pump beam, the pump beam generates free carriers through interband (d→sp) transitions. These carriers decay to the lower energy state through the intraband (sp→sp) transition and SPR decays within the conduction band. The probe beam is strongly absorbed when the sample is exposed to the pump beam, which also increases the creation of free carriers in the lower energy state. In this instance, the probe beam is in a "off" condition. When the sample is not exposed to the pump beam and the probe beam passes through the sample because of weak absorption of 633 nm, the output intensity is in "on" state. The sample behaves as an inverter switch.

The inverting switching was also observed with the pump beam wavelength at 514 nm for AuNPs. Different types of optical switching are reported in semiconductor nanocrystal solutions [32]. We are investigating the potential of these NPs for other logic gates such as AND, NOR, etc.

4. Conclusions

This work reports on the synthesis of AgNPs and AuNPs utilizing GA extract as a reducing and stabilizing agent. TEM, UV-Vis spectroscopy, and color changes verified the formation of the synthesized NPs. UV-Vis spectra revealed SPR bands with a single peak around 519 nm and 418 nm for AuNPs and AgNPs, respectively. According to TEM data, the NPs are spherical and have an average size of 4 nm for AuNPs and 5 nm for AgNPs. The diameters of the NPs were estimated using their absorption spectra, which were found to be in good agreement with the TEM data.

The nonlinear refraction (n_2) and absorption coefficient (β) of AuNPs and AgNPs at wavelengths of 488 nm and 514 nm were examined using the Z-scan technique. The nonlinear refractive index is believed to be caused by thermal effects, and the nonlinear absorption process occurs via Reverse Saturation Absorption (RSA). The mechanism of RSA is explained through interband, intraband transitions, and SPR decay. Optical limiting and optical switching are demonstrated by exploiting the nonlinear optical properties of the samples.

Overall, the paper demonstrates combining the eco-friendly synthesis of AuNPs and AgNPs using GA extract and studying the optical nonlinear properties and their use for optical limiting and optical switching. This study presents an efficient and sustainable method for the production of NPs with promising optical applications in advanced technology such as imaging, colourimetric sensors, plasmonic sensors, photothermal photodynamic therapies, and optoelectronic devices, for instance, solar cells, light-emitting diodes, and optical switching.

Ethical Statement

This study does not contain any studies with human or animal subjects performed by any of the authors.

Conflicts of Interest

The authors declare that they have no conflicts of interest to this work.

Data Availability Statement

Data are available from the corresponding author upon reasonable request.

Author Contribution Statement

Fryad Z. Henari: Conceptualization, Methodology, Software, Validation, Formal analysis, Investigation, Resources, Data curation, Writing – original draft, Writing – review & editing, Visualization, Supervision, Project administration. **G. Roshan Deen:** Conceptualization, Software, Formal analysis, Resources, Data curation, Visualization.

References

[1] Saylor, Y., & Irby, V. (2018). *Metal nanoparticles: Properties, synthesis and applications*. USA: Nova Science Publishers.

[2] Manaktala, S. S., & Singh, K. M. (2019). Optoelectronic devices-application of Nanotechnology – A review. *International Journal of Scientific & Engineering Research*, *10*(5), 54–60.

[3] Henari, F. Z., & Manaa, H. (2018). Nonlinear optical properties, optical limiting and optical switching of Ag nanoparticles prepared by a green synthetic method. *Optics and Photonics Journal*, *8*(07), 235. https://doi.org/10.4236/opj.2018.87020

[4] Indhu, A. R., Keerthana, L., & Dharmalingam, G. (2023). Plasmonic nanotechnology for photothermal applications – An evaluation. *Beilstein Journal of Nanotechnology*, *14*(1), 380–419. https://doi.org/10.3762/bjnano.14.33

[5] George, B. P., Chota, A., Sarbadhikary, P., & Abrahamse, H. (2022). Fundamentals and applications of metal nanoparticle-enhanced singlet oxygen generation for improved cancer photodynamic therapy. *Frontiers in Chemistry*, *10*, 964674. https://doi.org/10.3389/fchem.2022.964674

[6] Yusuf, A., Almotairy, A. R. Z., Henidi, H., Alshehri, O. Y., & Aldughaim, M. S. (2023). Nanoparticles as drug delivery systems: A review of the implication of nanoparticles' physicochemical properties on responses in biological systems. *Polymers*, *15*(7), 1596. https://doi.org/10.3390/polym15071596

[7] Dengler, S., Kübel, C., Schwenke, A., Ritt, G., & Eberle, B. (2012). Near-and off-resonant optical limiting properties of gold–silver alloy nanoparticles for intense nanosecond laser pulses. *Journal of Optics*, *14*(7), 075203. https://doi.org/10.1088/2040-8978/14/7/075203

[8] Yaqoob, A. A., Umar, K., & Ibrahim, M. N. M. (2020). Silver nanoparticles: Various methods of synthesis, size affecting factors and their potential applications – A review. *Applied Nanoscience*, *10*(5), 1369–1378. https://doi.org/10.1007/s13204-020-01318-w

[9] Lippitz, M., van Dijk, M. A., & Orrit, M. (2005). Third-harmonic generation from single gold nanoparticles. *Nano Letters*, *5*(4), 799–802. https://doi.org/10.1021/nl0502571

[10] Fathima, R., & Mujeeb, A. (2021). Nonlinear optical investigations of laser generated gold, silver and gold-silver alloy nanoparticles and optical limiting applications. *Journal of Alloys and Compounds*, *858*, 157667. https://doi.org/10.1016/j.jallcom.2020.157667

[11] Xu, J., Zhang, C., Wang, Y., Wang, M., Xu, Y., Wei, T., . . . , & Zhou, L. (2024). All-in-one, all-optical logic gates using liquid metal plasmon nonlinearity. *Nature Communications*, *15*(1), 1726. https://doi.org/10.1038/s41467-024-46014-3

[12] Dos Santos, O. A. L., Pizzorno Backx, B., Abumousa, R. A., & Bououdina, M. (2022). Environmental implications associated with the development of nanotechnology: From synthesis to disposal. *Nanomaterials*, *12*(23), 4319. https://doi.org/10.3390/nano12234319

[13] Jadoun, S., Arif, R., Jangid, N. K., & Meena, R. K. (2021). Green synthesis of nanoparticles using plant extracts: A review. *Environmental Chemistry Letters*, *19*(1), 355–374. https://doi.org/10.1007/s10311-020-01074-x

[14] Khalil, M. M., Ismail, E. H., El-Baghdady, K. Z., & Mohamed, D. (2014). Green synthesis of silver nanoparticles using olive leaf extract and its antibacterial activity. *Arabian Journal of Chemistry*, *7*(6), 1131–1139. https://doi.org/10.1016/j.arabjc.2013.04.007

[15] Deen, G. R., Hannan, F. A., Henari, F., & Akhtar, S. (2022). Effects of different parts of the okra plant (*Abelmoschus esculentus*) on the phytosynthesis of silver nanoparticles: Evaluation of synthesis conditions, nonlinear optical and antibacterial properties. *Nanomaterials*, *12*(23), 4174. https://doi.org/10.3390/nano12234174

[16] Madhusudhan, A., Reddy, G. B., & Krishana, I. M. (2019). Green synthesis of gold nanoparticles by using natural gums. In A. Husen & M. Iqbal (Eds.), *Nanomaterials and Plant Potential* (pp. 111–134) Springer. https://doi.org/10.1007/978-3-030-05569-1_4

[17] Eskandari-Nojehdehi, M., Jafarizadeh-Malmiri, H., & Jafarizad, A. (2018). Microwave accelerated green synthesis of gold nanoparticles using gum Arabic and their physico-chemical properties assessments. *Zeitschrift für Physikalische Chemie*, *232*(3), 325–343. https://doi.org/10.1515/zpch-2017-1001

[18] Djajadisastra, J., Sutriyo, P. P., & Pujiyanto, A. N. U. N. G. (2014). Antioxidant activity of gold nanoparticles using gum Arabic as a stabilising agent. *International Journal of Pharmacy and Pharmaceutical Science*, *6*(7), 462–465.

[19] Handayani, W., Ningrum, A. S., & Imawan, C. (2020). The role of pH in synthesis silver nanoparticles using pometia pinnata (matoa) leaves extract as bioreductor. *Journal of Physics: Conference Series*, *1428*(1), 012021. https://doi.org/10.1088/1742-6596/1428/1/012021

[20] Sheik-Bahae, M., Said, A. A., Wei, T. H., Hagan, D. J., & Van Stryland, E. W. (1990). Sensitive measurement of optical nonlinearities using a single beam. *IEEE Journal of Quantum Electronics*, *26*(4), 760–769. https://doi.org/10.1109/3.53394

[21] Srinath, B. S., & Ravishankar Rai, V. (2015). Biosynthesis of highly monodispersed, spherical gold nanoparticles of size 4–10 nm from spent cultures of *Klebsiella pneumoniae*. *3 Biotech*, *5*, 671–676. https://doi.org/10.1007/s13205-014-0265-2

[22] Haiss, W., Thanh, N. T., Aveyard, J., & Fernig, D. G. (2007). Determination of size and concentration of gold nanoparticles from UV−Vis spectra. *Analytical Chemistry*, *79*(11), 4215–4221. https://doi.org/10.1021/ac0702084

[23] Cuppo, F. L. S. A., Figueiredo Neto, A. M., Gómez, S. L., & Palffy-Muhoray, P. (2002). Thermal-lens model compared with the Sheik-Bahae formalism in interpreting Z-scan experiments on lyotropic liquid crystals. *Journal of the Optical Society of America B*, *19*(6), 1342–1348. https://doi.org/10.1364/JOSAB.19.001342

[24] Eslamifara, M., & Mansour, N. (2012). Optical limiting properties of colloids enhanced by gold nanoparticles based on thermal nonlinear refraction. *International Journal of Optics and Photonics*, *6*(1), 49.

[25] Sarkhosh, L., & Mansour, N. (2015). Analysis of Z-scan measurement for large thermal nonlinear refraction in gold nanoparticle colloid. *Journal of Nonlinear Optical Physics & Materials*, *24*(02), 1550014. https://doi.org/10.1142/S0218863515500149

[26] Fu, Y., Ganeev, R. A., Krishnendu, P. S., Zhou, C., Rao, K. S., & Guo, C. (2019). Size-dependent off-resonant nonlinear optical properties of gold nanoparticles and demonstration of efficient optical limiting. *Optical Materials Express*, *9*(3), 976–991. https://doi.org/10.1364/OME.9.000976

[27] Kelly, K. L., Coronado, E., Zhao, L. L., & Schatz, G. C. (2003). The optical properties of metal nanoparticles: The influence of size, shape, and dielectric environment. *The Journal of Physical Chemistry B*, *107*(3), 668–677. https://doi.org/10.1021/jp026731y

[28] Philip, R., Chantharasupawong, P., Qian, H., Jin, R., & Thomas, J. (2012). Evolution of nonlinear optical properties: From gold atomic clusters to plasmonic nanocrystals. *Nano Letters*, *12*(9), 4661–4667. https://doi.org/10.1021/nl301988v

[29] Mzwd, E., Alsaee, S. K., Suardi, N., Aziz, A. A., & Arshad, S. (2024). Exploring the nonlinear optical properties of gold nanoparticle colloids capped with Gum Arabic: A study utilising continuous wave laser and Z-scan technique. *Optical Materials*, *148*, 114907. http://dx.doi.org/10.2139/ssrn.4648540

[30] Alawfi, A. A., Henari, F. Z., Younis, A., & Manaa, H. (2020). Bio-inspired synthesis of silver nanoparticles using *Hibiscus Tiliaceus* L. flower extracts for improved optical characteristics. *Journal of Materials Science: Materials in Electronics*, *31*(23), 21073–21081. https://doi.org/10.1007/s10854-020-04619-6

[31] Pan, H., Chen, W., Feng, Y. P., Ji, W., & Lin, J. (2006). Optical limiting properties of metal nanowires. *Applied Physics Letters*, *88*(22), 223106. https://doi.org/10.1063/1.2208549

[32] Mukherjee, A., Saigal, N., & Pandey, A. (2019). Low power all optical switching and implementation of universal logic gates using micro-bubbles in semiconductor nanocrystal solutions. *Nanotechnology*, *31*(5), 055401. https://doi.org/10.1088/1361-6528/ab4f3b

How to Cite: Henari, F. Z., & Deen, G. R. (2024). Green Synthesis of Noble Metal Nanoparticles: Nonlinear Optics and Applications. *Journal of Optics and Photonics Research*. https://doi.org/10.47852/bonviewJOPR42023911